Intraseasonal and Interannual Variability of Mars' Present Climate

A NASA Ames Research Center Joint Research Interchange
Final Report

Jeffery L. Hollingsworth*†, Alison F. C. Bridger♭ & Robert M. Haberle†

University Consortium Agreement: NCC2-5094
Project Duration: 25 August 1994–24 February 1996

*San Jose State University Foundation, P.O. Box 720130, San Jose, California 95172, USA
†NASA Ames Research Center, MS: 245-3, Moffett Field, California 94035, USA
♭Department of Meteorology, San Jose State University, San Jose, California 95192, USA

ABSTRACT

This is a Final Report for a Joint Research Interchange (JRI) between NASA Ames Research Center and San Jose State University, Department of Meteorology. The focus of this JRI has been to investigate the nature of intraseasonal and interannual variability of Mars' present climate. We have applied a three-dimensional climate model based on the full hydrostatic primitive equations to determine the spatial, but primarily, the temporal structures of the planet's large-scale circulation as it evolves during a given seasonal advance, and, over multi-annual cycles. The particular climate model applies simplified physical parameterizations and is computationally efficient. It could thus easily be integrated in a perpetual season or advancing season configuration, as well as over many Mars years. We have assessed both high and low-frequency components of the circulation (i.e., motions having periods of $\mathcal{O}$(2–10 days) or greater than $\mathcal{O}$(10 days), respectively). Results from this investigation have explored the basic issue whether Mars' climate system is naturally 'chaotic' associated with nonlinear interactions of the large-scale circulation—regardless of any allowance for year-to-year variations in external forcing mechanisms. Titles of papers presented at scientific conferences and a manuscript to be submitted to the scientific literature are provided. An overview of a areas for further investigation is also presented.

1. INTRODUCTION

Fluctuations in a planet's atmospheric circulation are either *internal* in nature, caused by intrinsic instability of the flow and by interactions between different types of motions; or *external* in origin, caused by variations in imposed external parameters (e.g., variations in incident solar radiation with a planet's orbit or coupling between surface fields (e.g., topography, polar ice caps) and the atmosphere [1,2]. Fundamental questions related to a planet's climate are: Which process is responsible for the strongest long-period variability? And, what is the nature of the interactions between the two kinds of fluctuations?

Over a range of spatial and temporal scales, Mars' atmosphere, as Earth's, exhibits substantial variations in its field variables (e.g., temperature and momentum) and trace constituents (e.g., water vapor and dust). The spatial and temporal variations can be associated with a wide variety of internal and external physical processes within its atmosphere [3,4]. Analyses of Viking lander surface-pressure data have indicated definitive evidence for specific meteorological signals such as thermal tides [5] and recurrent midlatitude weather systems (i.e., transient baroclinic eddies) [6,7]. However a complete observational database of global meteorological variables, in particular their variations during a seasonal cycle and from year-to-year, does not presently exist for Mars. One must therefore resort to other means to infer aspects of the planet's global circulation patterns and climate. One such method is the application of atmospheric dynamical models.

By far the most sophisticated models are general circulation models (GCMs). These models include detailed formulations of atmospheric flow dynamics based on the meteorological primitive equations; they also include complex physics for 'right hand side' terms in the governing system of equations (e.g., radiative-transfer physics to yield diabatic heating rates). GCMs are thus computationally intensive. Another approach is to simplify the physics without compromising the flow dynamics. This is a so called 'simple physics' primitive equations (SPPE) model. SPPE models are efficient 'mechanistic' tools that can be used to examine particular components of the atmospheric circulation (e.g., the zonally symmetric circulation, the transient circulation and the stationary circulation) and their mutual interactions. They are also useful in performing parameter sensitivity studies (e.g., determining the sensitivity to thermal relaxation and momentum dissipation strengths). And because computations related to the external physics are minimized, SPPE models are effective numerical models for performing multi-annual simulations which can be used to address questions related to long-term internally or externally driven climate variability.

We have adapted the SPPE model of [8] to investigate aspects of Mars' atmospheric circulation and the nature of its present climate. The Mars climate model (MCM) uses simplified physical parameterizations: diabatic heating is specified in terms of a meridionally dependent thermal relaxation (Newtonian cooling) towards a 'radiative-equilibrium' temperature field, and momentum drag is specified in terms of a height-dependent drag (Rayleigh friction). A prescribed zonally symmetric radiative-equilibrium thermal field as a function of latitude, height and season is independently determined using results from a 1-D radiative-convective model. The MCM uses a spectral (spherical harmonic) representation in the horizontal and finite differences in the vertical for computations of the dependent variables. The seasonal condensation of CO_2 onto the polar caps is also included with a parameterization.

The MCM has been used successfully to investigate key components of Mars' atmospheric circulation, for example, its zonally symmetric (Hadley) circulation and its midlatitude thermally indirect (Ferrel) circulation [9]. Driven by large-scale traveling weather systems (i.e., transient barotropic and/or baroclinic eddies) which grow and decay within the rapidly rotating, intrinsically unstable atmosphere, this latter extratropical circulation is a key agent in the transport of heat and momentum [10] and particular to Mars, volatiles and dust [4]. In many aspects, the MCM shows qualitatively and quantitatively similar structures of the global circulation as in the fully complex Mars general circulation model (MGCM) used at NASA Ames [11,12,13]. Yet because of its simple physics parameterizations, the MCM is more ideally suited to perform multi-annual simulations aimed at addressing questions related to internally or externally driven variability of Mars' long-term climate.

2. KEY RESULTS OF INVESTIGATION

The primary objectives of this research were: (a) to examine both high and low-frequency spatial and temporal structures of mean and eddy statistics from simulations of Mars' atmospheric circulation; and, (b) to examine the degree and significance of intraseasonal and interannual (i.e., ultra-low frequency) variability of the planet's current climate. Both objectives were addressed using the computationally efficient, three-dimensional Mars climate model described above. By 'high', 'low' and 'ultra-low' frequency, it is meant atmospheric circulation components with periods of $\mathcal{O}$(2–10 days), $\mathcal{O}$(10–100 days) and $\mathcal{O}$(1–10 years), respectively. By 'mean' and 'eddy' it is meant a time and/or zonal average, and the departures therefrom. By 'intraseasonal' and 'interannual' variability it is meant significant circulation changes within a given seasonal progression (e.g., fall through spring in the northern hemisphere) and variations in such changes from year-to-year, and significant year-to-year departures of particular mean and eddy statistics of the circulation, respectively.

a. Multi-annual simulations: interannual variability

A total of 60 Mars years in a 'coarse' configuration (i.e., 'trapezoidal' spherical harmonic truncation 16Tr06 and 14 vertical layers) with no topography nor CO_2 condensation cycle have been simulated using the MCM. From such a long integration, a realistic data set has been produced to investigate variability of the circulation and climate on intraseasonal and interannual time scales. Absence of complex external forcings (e.g., realistic solar/IR radiation and surface variations) permits internally generated (i.e., nonlinear) variability of the climate system to be examined in isolation. The predominant external forcing in this version of the MCM is the radiative relaxation applied to drive the climate through its annual cycle. It also imposes the longest time scale on the system. Any variability seen on longer time scales is thus generated internally.

Even in the absence of realistic external forcings (e.g., enhanced thermal radiation accompanying high dust loading or large-scale flow interaction with spatially varying surface topography), the long-term simulation has indicated significant interannual variability, with the greatest variations occurring in the southern hemisphere (SH) during late winter and spring seasons. The variability of the circulation has been assessed by examination of hemispherically integrated zonal and eddy kinetic energies (ZKE and EKE, respectively [14]).

Figure 1 shows an example of year-to-year variations in the northern hemisphere (NH) mean zonal kinetic energy as a function of season for the first 10 years of the 60 year simulation. The ZKE in the NH peaks during winter ($L_s = 270°$) associated with a vigorous circumpolar westerly jet and is weak during summer and fall ($L_s = 90$–$140°$) when an easterly jet dominates. In contrast as shown in Figure 2, the ZKE in the SH shows a dual peak, with the first peak during southern winter ($L_s = 90°$) accompanying the SH westerly jet during this season and the second (larger) peak just prior to southern spring equinox ($L_s = 140$–$180°$). As can be seen from the annual cycle's nonuniform spread in the years depicted in both Figures 1 and 2, there is evidence of nontrivial year-to-year variations in the mean zonal kinetic energy of both hemispheres. Furthermore, there is also significant asymmetry in the annual cycle between northern and southern hemispheres.

The eddy kinetic energy associated with the midlatitude transient eddies is not only significantly weaker than the zonal kinetic energy, it also exhibits larger year-to-year variability. Figure 3 shows the EKE in the SH as a function of season and its variation during the first 10 years. During southern winter, the transient eddies are surprisingly weak, much weaker than

their counterparts during northern winter. Similar weak transient-eddy activity has been found in the NASA Ames MGCM [13]. It appears that the weak activity is, in part, independent of the details of zonally symmetric or asymmetric surface forcings (e.g., large-scale topography). Other internal processes must be important. However, SH eddy activity rises dramatically during spring and is far greater than that in the north at any season. A similar seasonal pattern as seen in Figure 3 is apparent for the NH transient eddies yet the fluctuations are much less pronounced. This year-to-year variability in SH winter transient eddy activity occurs in a model with simple but repeatable forcing. And it therefore suggests that Mars' climate system has sufficient nonlinearity to produce interannual variability regardless of specific details of the imposed external forcing.

A 1-day 'snap shot' of the transient-eddy activity or 'weather' as simulated by the MCM is indicated in Figure 4. The particular season chosen corresponds to northern spring where eddies are active in both hemispheres. At this level in the atmosphere (roughly 20 km), the eddy geopotential shows a series of high and low centers in the middle latitudes with a dominant wavenumber-3 pattern. The latitudinal band of the centers of these weather systems (i.e., ± 50–$60°$) corresponds to active 'storm belts' [15] on Mars during this season.

We have also examined time series from the MCM grid point nearest the Viking Lander 2 (VL2) site for long-term variability (in the present model configuration, this is at 126 deg E, 47 deg N, 0.3 km). As seen in Figure 5, the 60-year record of once daily (instantaneous) temperature shows a 'red noise' spectrum characteristic of geophysical time series, with a marked increase in spectral power toward the lowest frequencies [1,16] here, out to the decadal time scales. The annual, semi-annual and sub-annual harmonics exhibit the greatest power, and a hint of variability on time-scales larger than the annual-cycle can also be seen. Moreover, considerable variability in the 10–100 day range and 2–0 day range is apparent, which is associated with low-frequency wave activity on intraseasonal time scales [15] and the passage of developing and decaying weather cyclones (i.e., day-to-day fluctuations), respectively, over the sample grid point. The latter eddy activity occurs in the midlatitude storm belt mentioned earlier and can be highly modulated by the presence of Mars' continental-scale orography [17]. Such effects are not present in the current version of the MCM. The low-frequency variations of the atmospheric circulation are not present merely at this particular grid point. Sample power spectra of a daily time series constructed by vertically integrating the mean equator-to-pole temperature difference exhibit very similar dominant spectral peaks and variability.

b. Multi-annual simulations: intraseasonal variability

In order to systematically analyze any 'noisy' circulation time series produced by the MCM, and the statistical significance of the results, we have applied useful analysis tools originally developed for Earth atmospheric studies to the climate model. Singular spectrum analysis (SSA) has been used to improve the determination of spectral estimates and to isolate statistically significant spectral power [16,18]. Essentially, SSA is an optimal-adaptive filtering technique; when used in combination with low-order maximum entropy (i.e., autoregressive) models (MEM), SSA is very effective in isolating dominant periods of motions when the background noise may be 'white' [16].

To assess, for example, the dominant periods of motion in the circulation over an intraseasonal time scale, and moreover, any significant variability in such periods from year to year, SSA can be used on a subset of a multi-year time series. Below we demonstrate the technique using a time series from the climate model multi-annual simulation.

For the sample VL2 grid point of the MCM, a time series during northern late fall through early spring ($L_s = 247$–$348°$) from year 38 of the 60-year MCM run has been extracted. This particular section of the time record is shown in Figure 6. Prior to analysis, the seasonal-mean has been removed and the time series has been 'centered' about the mean. The noisy curve in Figure 6 represents the 'raw' time series and the smooth curve the 'best fit' using the adaptive filtering technique. The best fit curve was derived from a projection of the original time series upon an optimal set of basis functions (i.e., temporal empirical orthogonal functions, or T-EOFs) as discussed in *Penland et al.* [16]. The amplitudes of each 'harmonic' of this optimal projection (i.e., temporal principal components, or T-PCs) are ordered descendantly and each explains a decreasing amount of the time series' total variance. Figure 7 shows a plot of the first 20 eigenvalues determined by this technique associated with the raw time series shown in Figure 6. The first 5 eigenvalues explain approximately 97.9% of the variance of the raw series. For more completeness, in the construction of the smoothed curve shown in Figure 6 we have retained eigenvalues (T-EOFs) and eigenfunctions (T-EOFs) 1–8.

An anomaly time series can then be constructed by subtracting the fitted from the raw time series and this subsequently analyzed spectrally using the MEM method. Figure 8 shows the anomaly time series for the northern late fall through early spring season for this particular year of the multi-annual simulation. In the anomaly time series, a 3–4 day oscillation is apparent which is 'enveloped' with an oscillation of much longer period, one in the range of $\mathcal{O}$(30–50 days). The question arises then which are the dominant periods in this sample time series. Applying a low-order MEM to determine the dominant periods, the sample power spectra shown in Figure 9 is obtained. The particular MEM algorithm used in this estimate is a 10-pole autoregressive model [16]. During the northern winter season (within this particular year), it is found that the dominant periods are 2.6, 3.4, 6.6 and 10.6 days. These spectral peaks are robust and are reproducible using independent estimates of the power (e.g., multi-tapper methods (MTM) as described in *Dettinger et al.* [18] with 90% statistical significance using an F-test). Such periods are associated with the transient baroclinic/barotropic eddies in the sub- and extratropics (i.e., weather systems similar in spatial structure to those depicted in Figure 4), and they correspond to the dominant modes inherent in this time signal of the seasonal progression (Figure 6).

Applying the same SSA technique for the same (or different) seasons, and for several years of the multi-annual time record, we can examine the dominant modes and their fluctuations and thereby detect with confidence any year-to-year variability in the simulation on intraseasonal time scales.

3. PRESENTATIONS AND PUBLICATIONS

Preliminary results on the seasonal asymmetries of the transient eddies and on interannual variability were presented at a scientific conference. And a manuscript is in preparation based on research results obtained during the period of this JRI which will be submitted to the scientific literature. Titles for these contributions are:

Hollingsworth, J.L., R.M. Haberle, H.C. Houben, and R.E. Young, 1994: Annual-cycle simulations using a Mars climate model. *Annales Geophysicae*, **12**, C656.

Hollingsworth, J.L., R.M. Haberle, H.C. Houben, and R.E. Young, 1996: Intraseasonal and interannual variability of Mars' climate in a simple global circulation model. To be submitted to: *Icarus*

4. DISCUSSION AND AREAS FOR FUTURE WORK

Understanding the dynamical mechanisms responsible for the rise and fall of the transient eddy activity during seasonal advance, the hemispheric asymmetries in mean and eddy energetics of the circulation, the sensitivity to realistic albeit mechanistic external forcings, and the influences each has on the intraseasonal and interannual variability of Mars' climate are topics we have begun to investigate under this research agreement. We have, nevertheless, only analyzed a small subset of our long-time record from the 60-year simulation. We outline below areas for further investigation related to intraseasonal variability for other periods, variability under enhanced dust loadings, and other potential measures of interannual variability.

a. Multi-annual simulations: enhanced dust opacities and imposed dust cycle

Isolating fundamental causes of Mars' climate variability while the 'system' (i.e., atmosphere and surface interface) is forced at the annual frequency under both low and quasi-periodic enhanced dust loadings, could be examined mechanistically with the coupled MCM. Though there is ample evidence that a preferred seasonality exists when planet-encircling storms are generated, it is recognized that the global storms occur intermittently on a year-to-year basis [19]. *Ingersoll and Lyons* [20] argued using a simplified two-parameter dust-circulation model that a possible source for interannual variability is the dust loading itself (i.e., an external forcing). Assuming equal time scales for dust raising and dust storm decay, aperiodic solutions were found for a wide range of parameter choices. Whether realistic Mars climate models such as the MCM show naturally 'chaotic' solutions in multi-annual simulations, without year-to-year variations in external forcings (e.g., regional versus global atmospheric dustiness), should be investigated. Chaotic signatures (i.e., 'red' power spectra) may arise solely associated with the nonlinearity of the governing flow equations. Yet it may also be associated with interactions between a forced, steady circulation and the life cycles of the transient eddies [1,21].

Long-term perpetual-season, as well as multi-annual simulations should be performed with a modified version of the MCM that incorporates realistic large-scale surface topography. The experiments performed to date do not include topographic effects. Originally, we had planned to include topography in the MCM; however, the required code modifications and necessary model testing proved to be formidable. Under this agreement, we therefore decided to examine long-term circulation statistics using the simpler lower boundary condition exclusively. Conceivably, 60–100 years of time integration should be performed with a topography version of the MCM in order to detect with confidence the low-frequency, annual and decadal time-scale variability in these simulations. A small suite of simulations will be carried out for the annual-cycle having

- idealized topography (i.e., hemispherically isolated mountains)
- a CO_2 condensation cycle
- enhanced dust loading (i.e., dusty radiative equilibrium temperatures and relaxation rates)
- a Viking Lander-like dust opacity cycle

b. Low-frequency variability: spatial structures

Further investigation on the dynamical mechanisms responsible for the relative minimum found in the integrated EKE near winter solstice in the simulations without topography should

be pursued. Namely, can barotropic/baroclinic competition [22] occur prior to solstice as is the case in the Earth's atmosphere? Whether such extrema and seasonal asymmetry occur when realistic orography is included in the MCM should also be examined. Analyses of mean and eddy fields in terms of a transformed Eulerian mean (TEM) formulation of the energy cycle [23] should be also carried out. This alternative formulation has the advantage that there is a more direct description of the eddy-to-mean and kinetic-to-potential interactions near the nonacceleration limit.

Separation of the temporal and spatial scales of the atmospheric circulation, its low frequency variability, and spatial patterns of such variability requires care. We suggest extending our methods discussed above and performing 1-point correlation analyses from time-filtered time series of the simulations to determine whether 'teleconnection' patterns, analogous to the 'Pacific-North American' (PNA) or 'North Atlantic Oscillation' (NAO) patterns seen in the terrestrial northern winter atmosphere [14] may occur in atmospheric circulation fields for Mars. On Earth, these patterns indicate connections between low-frequency transients in low and middle latitudes and can be associated with meridionally propagating Rossby waves [2]. Alternatively, one could judiciously pick out the spatial structure of the variability (essentially, similar to SSA methods for temporal variability) in terms of empirical orthogonal function (EOF) analysis [14,24]. The principal advantage of EOF analysis is that it provides an extremely efficient way to describe geophysical data in both space and time. From time series taken from several observational points, a covariance eigenvector/eigenvalue problem is constructed. In this formulation the eigenvectors (i.e., EOFs) correspond to the spatial structure of the variability of the field variables and the eigenvalues (i.e., principal components) are newly generated time series which explain a known percentage of the variability associated with each EOF. EOF analysis would be particularly useful in identifying any 85-day intraseasonal extratropical oscillation proposed by *Keppenne* [25] and in capturing its spatial structure.

REFERENCES

1. James, I. N., and P. M. James, 1992: *Quart. J. Roy. Meteor. Soc.*, **118,** 1211–1233.
2. James, I. N., 1994: *Introduction to Circulating Atmospheres*, (Cambridge Univ. Press., Cambridge).
3. Leovy, C. B., 1985: *Adv. Geophys.* **28,** Part A, 327–346.
4. Zurek, R. W., et al., 1992: in *Mars*, H. H. Kieffer, B. M. Jakosky, C. W. Snyder, and M. S. Matthews, Eds., (Univ. Arizona Press, Tucson), 835–933.
5. Leovy, C. B., and R. W. Zurek, 1979: *J. Geophys. Res.*, **84,** 2956–2968.
6. Barnes, J. R., 1980: *J. Atmos. Sci.*, **37,** 2002–2015.
7. Barnes, J. R., 1981: *J. Atmos. Sci.*, **38,** 225–234.
8. Young, R. E. and G. L. Villere, 1985: *J. Atmos. Sci.*, **42,** 1991–2006.
9. Haberle, R. M., H. Houben, R. E. Young, and J. R. Barnes, 1996: (Submitted to *J. Geophys. Res.*).
10. Hoskins, B. J., et al., 1983: *J. Atmos. Sci.*, **40,** 1595–1612.
11. Pollack, J. B., et al., 1990: *J. Geophys. Res.*, **95,** 1447–1474.
12. Haberle, R. M., et al., 1993: *J. Geophys. Res.*, **98,** 3093–3124.
13. Barnes, J. R., et al., 1993: *J. Geophys. Res.*, **98,** 3125–3148.
14. Peixoto, J. P., and A. H. Oort, 1992: *Physics of Climate*, (American Institute of Physics, New York).
15. Grotjahn, R., 1993: *Global Atmospheric Circulations: Observations and Theories*, (Oxford Univ. Press, New York).
16. Penland, C., M. Ghil, and K. M. Weickmann, 1991: *J. Geophys. Res.*, **96,** 22659–22671.
17. Hollingsworth, J. L., et al., 1996: *Nature*, **380,** 413–416.
18. Dettinger, M. D., et al., 1995: *Eos, Trans. American Geophysical Union*, 76, 12, 14, 21.
19. Zurek, R. W., and L. J. Martin, 1993: *J. Geophys. Res.*, **98,** 3247–3259.
20. Ingersoll, A. P., and J. R. Lyons, 1993: *J. Geophys. Res.*, **98,** 10951–10961.
21. James, P. M., I. N. James and K. Fraedrich, 1994: *Quart. J. Roy. Meteor. Soc.*, **120,** 1045–1067.
22. James, I. N., 1987: *J. Atmos. Sci.*, **44,** 3710–3720.
23. Plumb, R. A., 1983: *J. Atmos. Sci.*, **40,** 1669–1688.
24. Horel, J. D., 1981: *Mon. Wea. Rev.*, **109,** 2080–2092.
25. Keppenne, C. L., 1992: *Icarus*, **100,** 598–607.

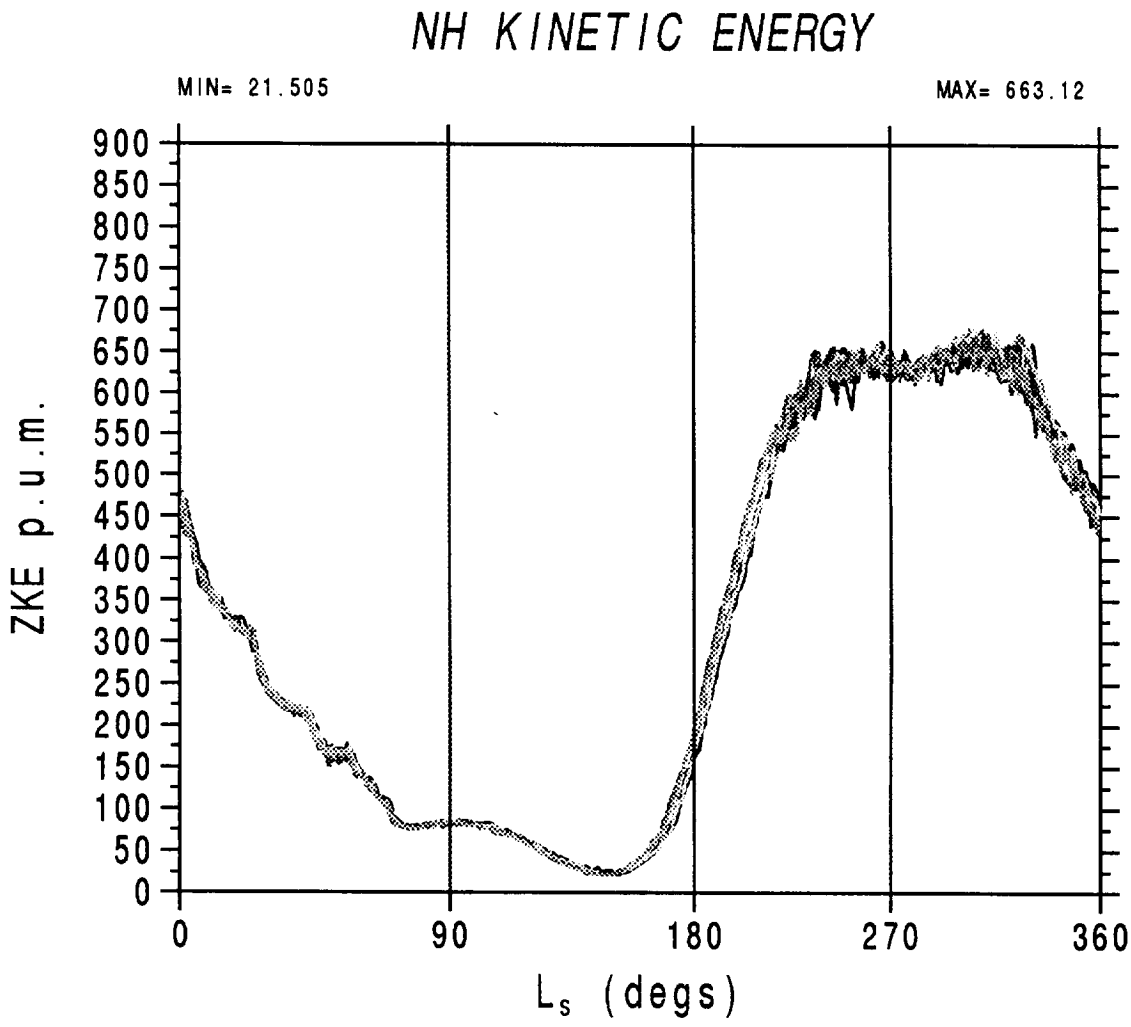

Figure 1: Vertically and hemispherically averaged mean zonal kinetic energy ($m^2\ s^{-2}$) as a function of season (L_s) for the northern hemisphere for the first 10 years of a 60-year simulation with the Mars climate model (MCM). The zonal kinetic energy (ZKE) is computed from the instantaneous (once daily), longitudinally averaged horizontal wind components (i.e., north-south, east-west) at all model levels.

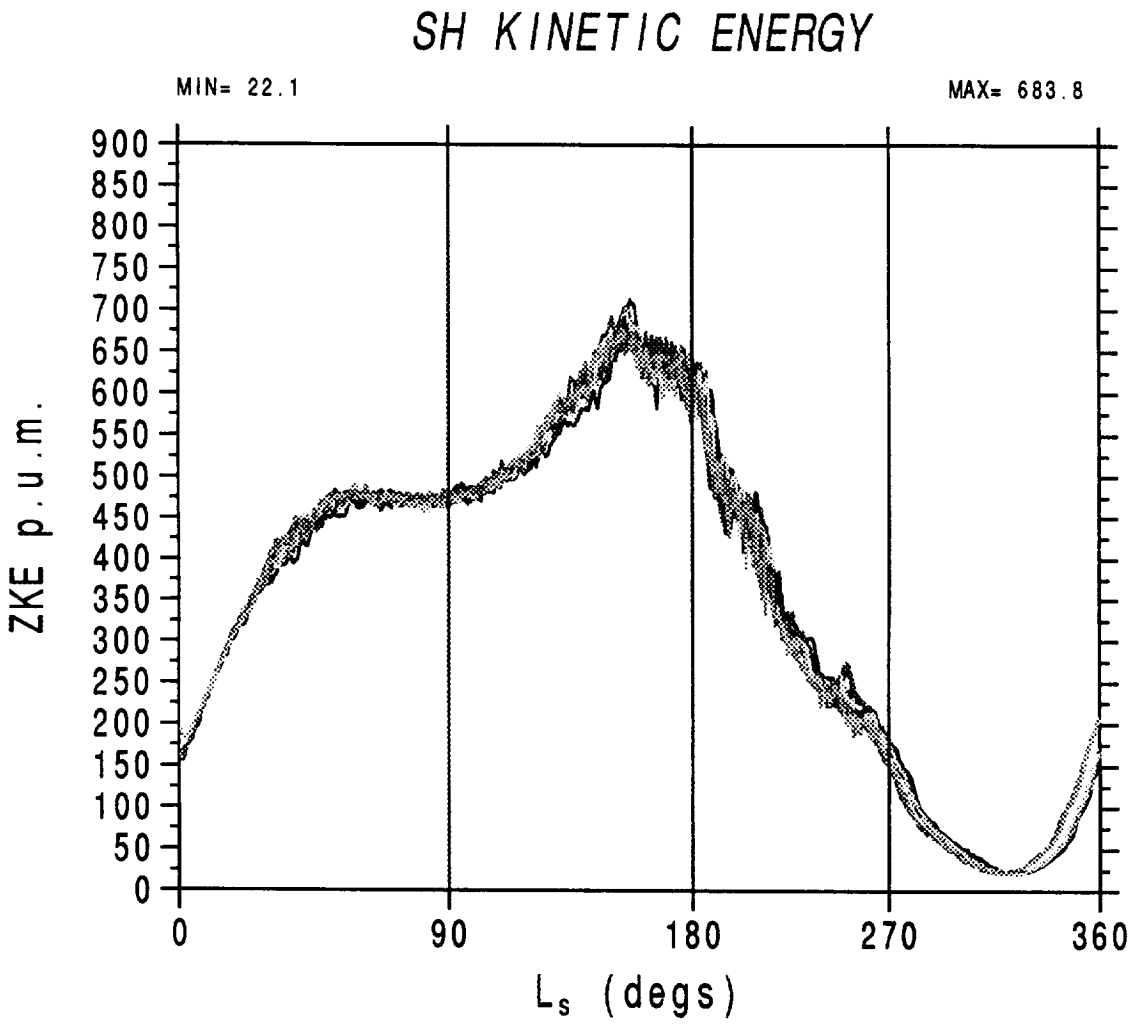

Figure 2: As in Figure 1 but for the southern hemisphere.

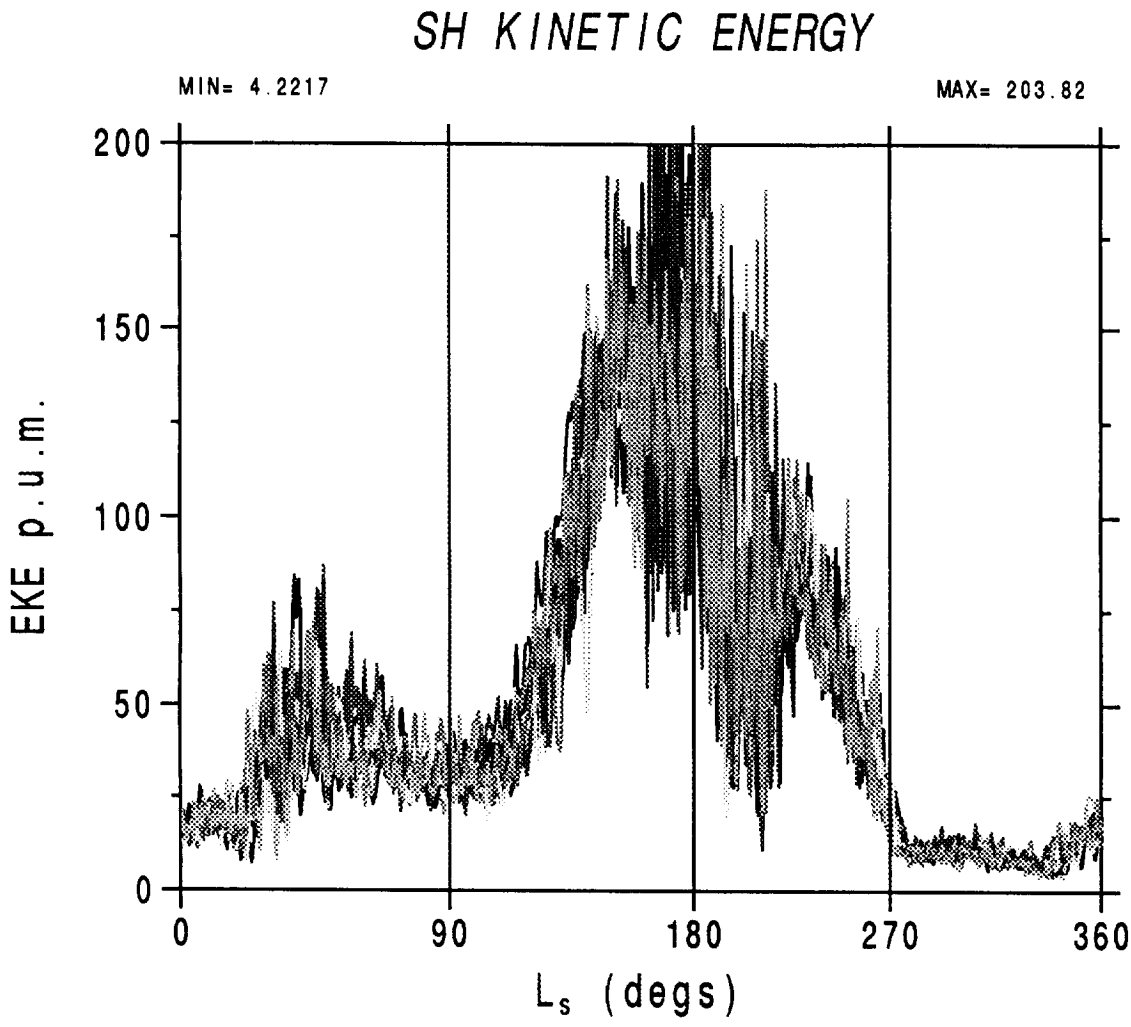

Figure 3: As in Figure 2 but for the vertically and hemispherically averaged transient-eddy kinetic energy ($m^2\ s^{-2}$). The eddy kinetic energy (EKE) is computed from the instantaneous departures (once daily) of the horizontal wind components (i.e., north-south, east-west) from the zonal (longitudinal) means at all model levels.

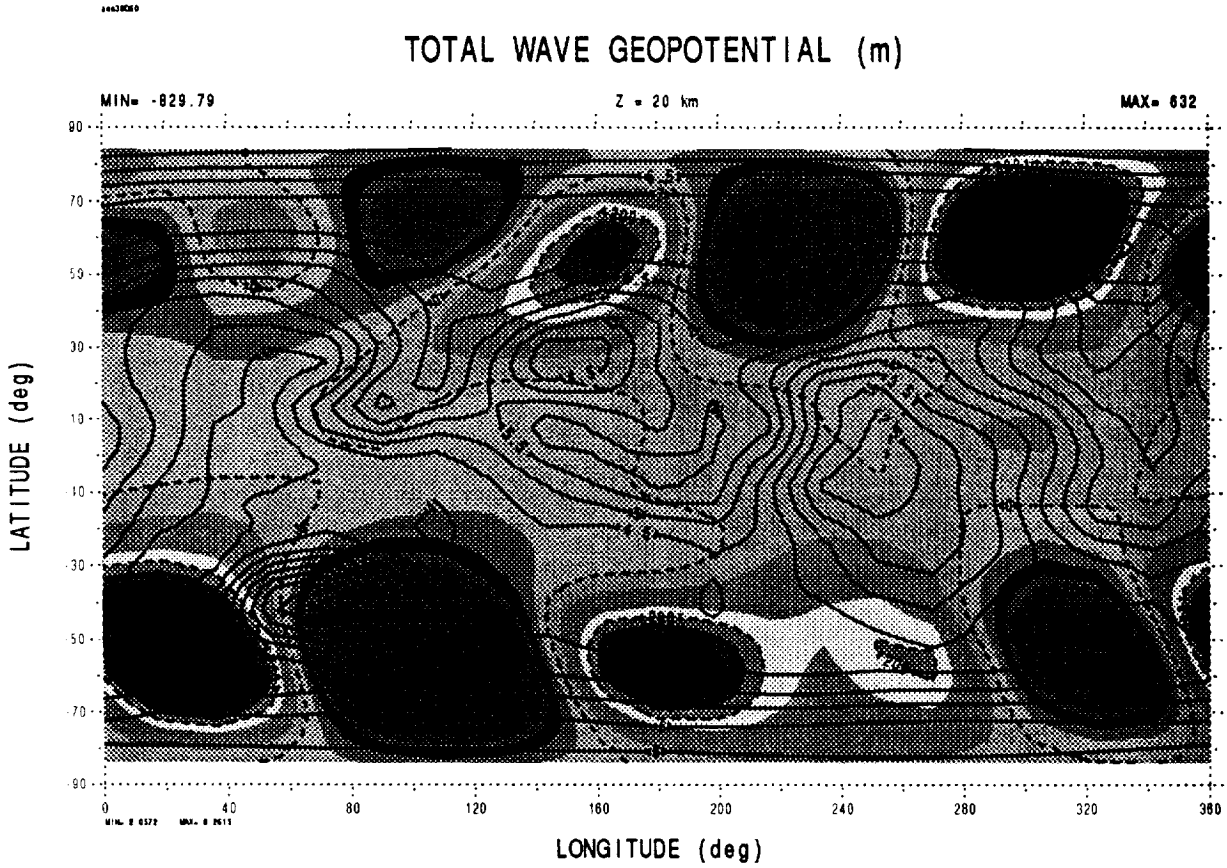

Figure 4: A longitude-latitude map of a 1-day 'snap shot' of transient-eddy activity or 'weather' as simulated at the 20-km level during northern spring season ($L_s = 30°$). The shaded regions with dashed contours correspond to high and low eddy geopotential (m) on day 60 from year 38 ($L_s = 0°$ corresponds to day 1). As a reference, the solid contours correspond to an average surface pressure distribution (mb) which highlights Mars' primary large-scale geographic features (e.g., Tharsis, Elysium, Arabia and Hellas). In this version of the MCM, however, a flat surface topography is used.

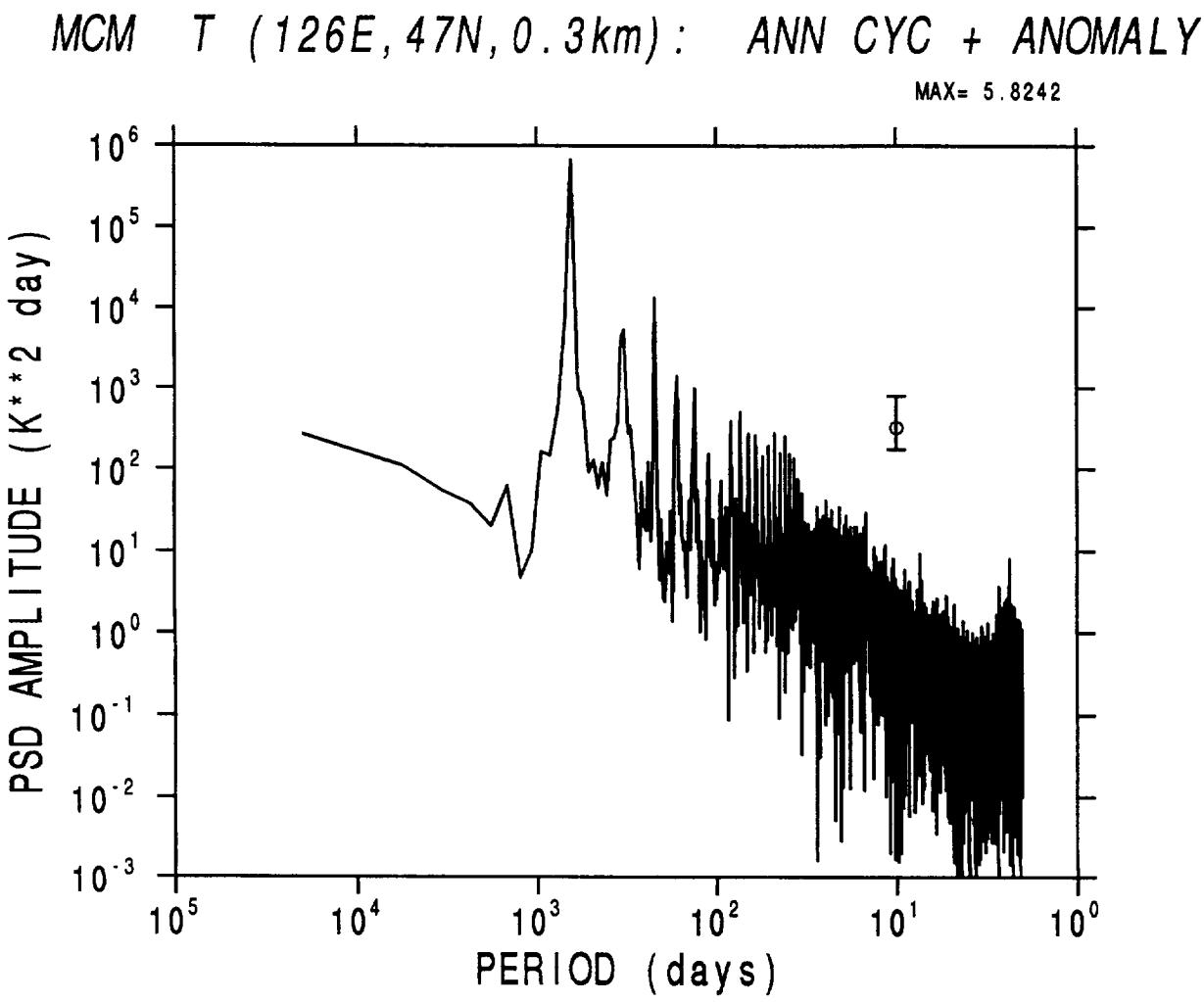

Figure 5: Band-averaged power density spectrum (K^2 day) computed from a 60-year temperature time series (sampled once daily) from the MCM grid point nearest the Viking Lander 2 (VL2) site. (For the multi-year integrations in the specified model resolution, this grid point corresponds to 126° E, 47° N, and 0.3 km.) Prior to application of the FFT, the time series was band averaged into bins having a width of 5 days. The 90% confidence limits on the band-averaged spectral estimates using a Chi-square distribution and 10 degrees of freedom is indicated by the error bar.

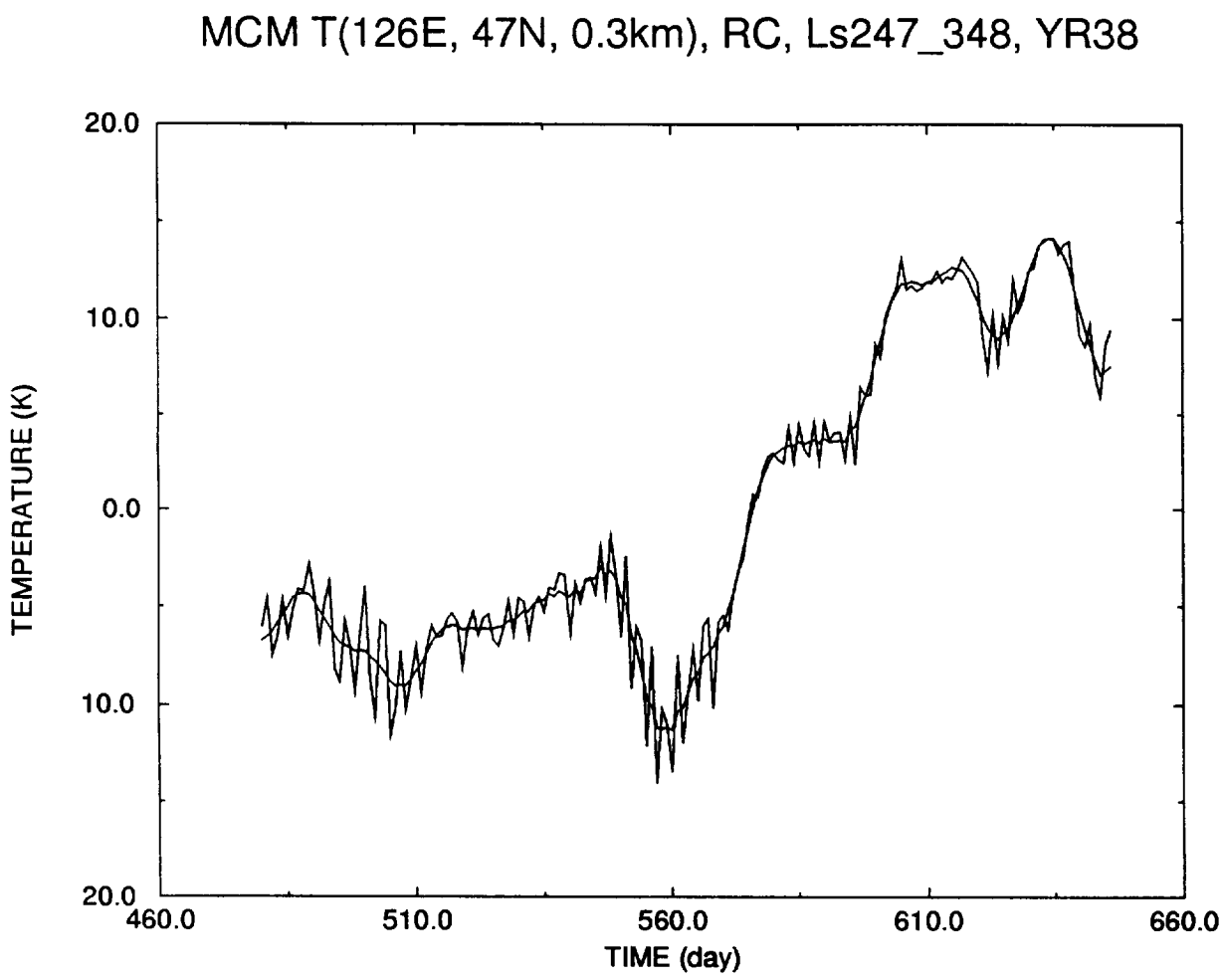

Figure 6: Singular spectrum analysis (SSA) on a segment of the long time series applied in Figure 5 (from simulated year 38 of the 60-year simulation) that corresponds to northern late fall through early spring ($L_s = 247\text{–}348°$). Shown are the 'raw' temperature (K) time series (noisy curve) and 'best fit' (smooth curve) determined using the adaptive filtering technique of SSA. Prior to SSA, the seasonal-mean was removed and the time series was centered about the mean. In this particular SSA model, a window of width 20 was used and the first 8 significant eigenvalues (temporal principal components, or T-PCs) and eigenfunctions (temporal empirical orthogonal functions, or T-EOFs) as described in *Penland et al.* [1991] were retained.

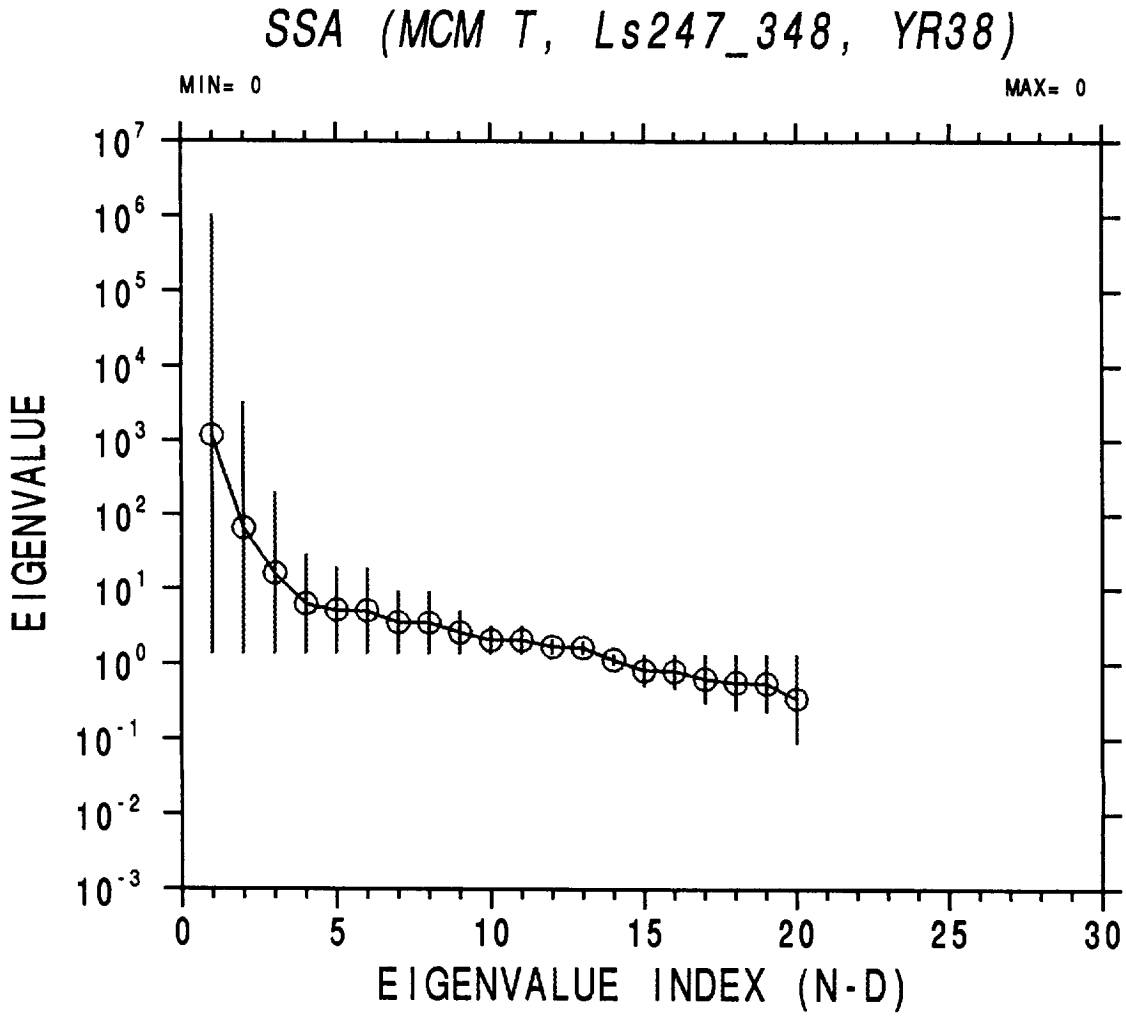

Figure 7: The first 20 eigenvalues of the centered raw time series shown in Figure 6. Eigenvalues 1-5 explain 97.9% of the variance.

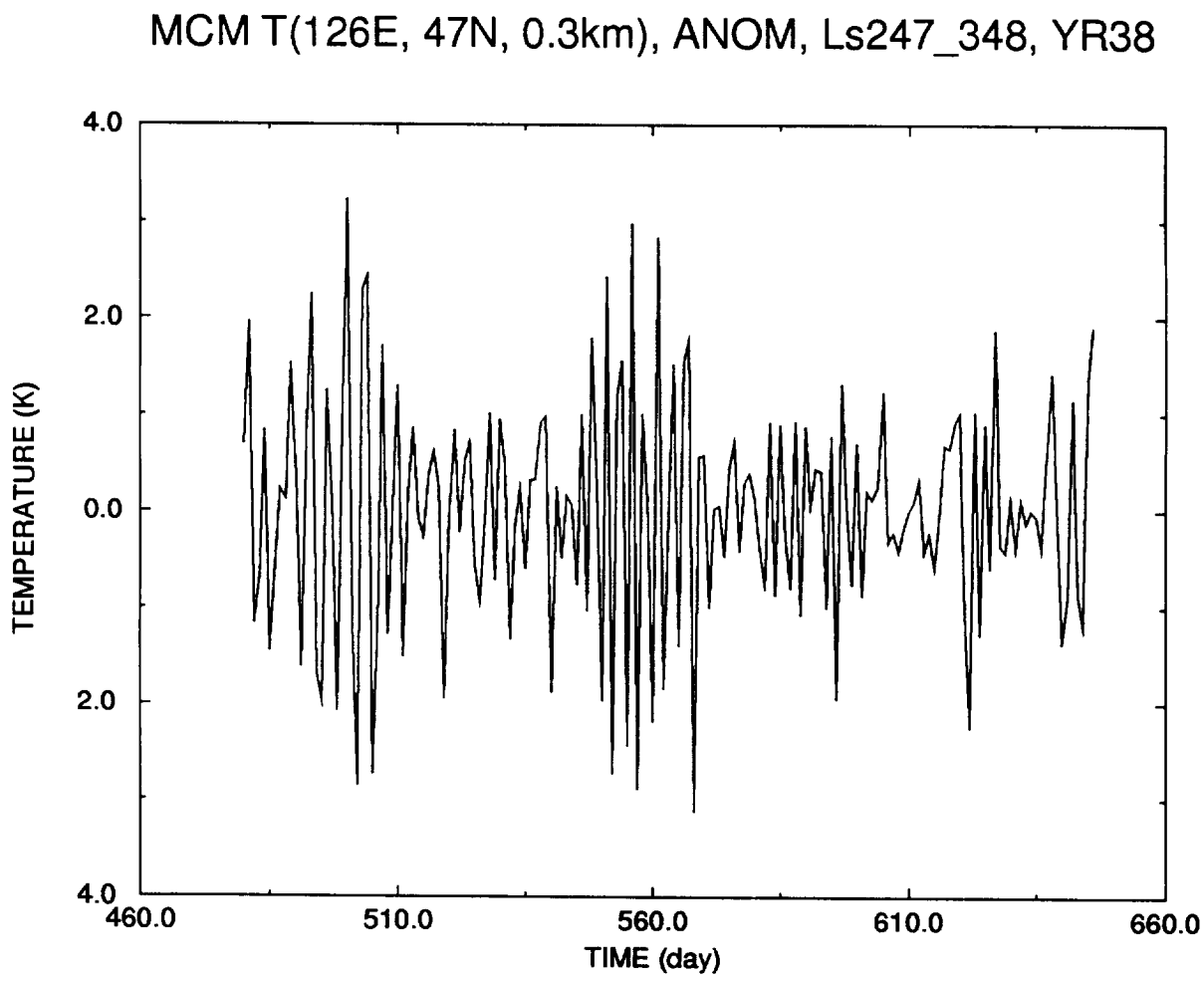

Figure 8: The 'anomaly' temperature (K) time series formed by subtracting the best fit from the raw time series shown in Figure 6.

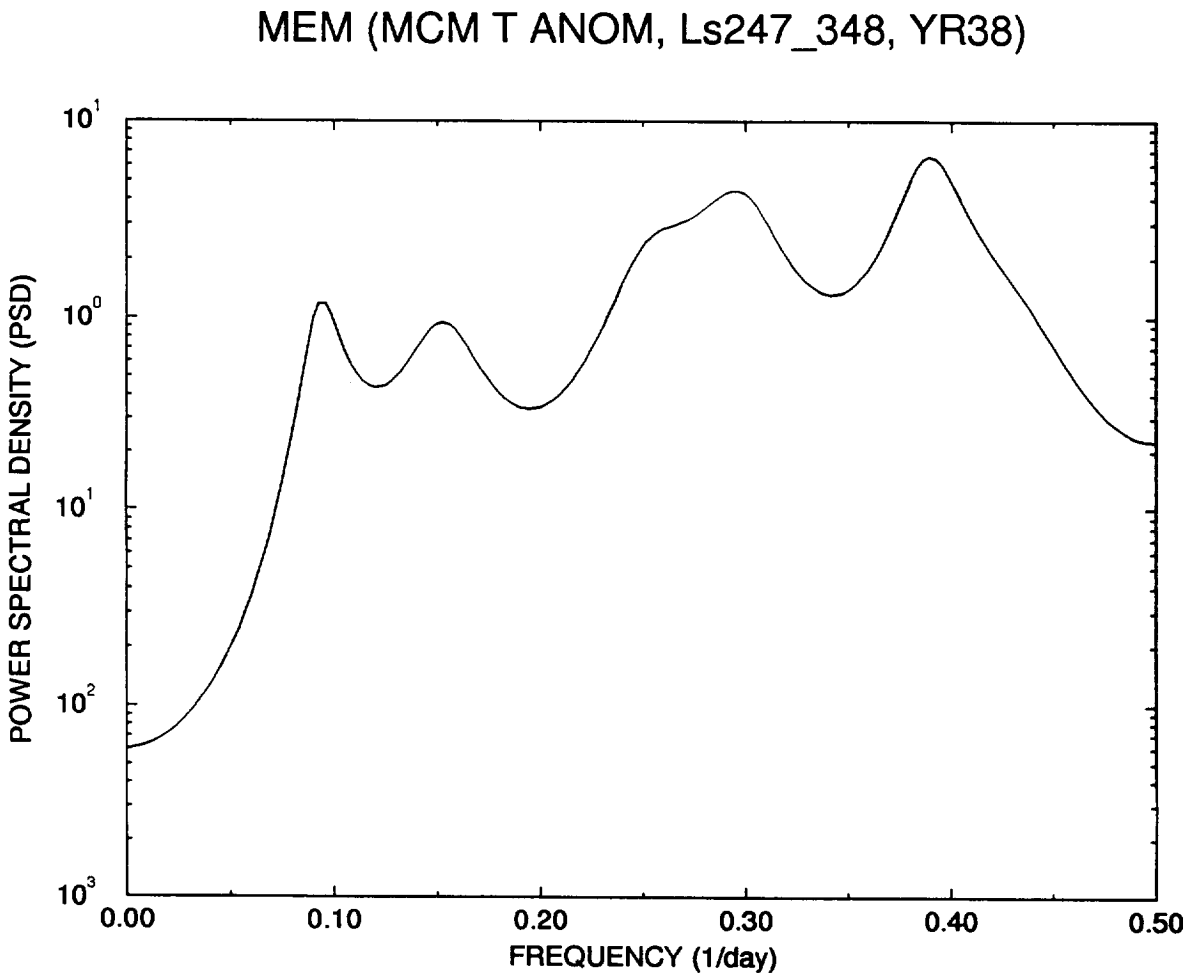

Figure 9: Power spectral density estimates from the maximum entropy method (MEM) using 10 poles in the autoregressive (AR) model [*Penland et al.*, 1991] of the anomaly time series shown in Figure 8. The spectral peaks are robust and are reproducible using independent estimates of the power (e.g., multi-tapper methods (MTM) as described in *Dettinger et al.* [1995] with 90% statistical significance using an F-test).